Full Text View

Volume 28, Issue 6 (June 1998)

Journal of Physical Oceanography
Article: pp. 1152–1172 | Abstract | PDF (1.01M)

Barotropic Response of the Labrador/Newfoundland Shelf to a Moving Storm

C. L. Tang

Bedford Institute of Oceanography, Ocean Sciences Division, Department of Fisheries and Oceans, Dartmouth, Nova Scotia, Canada

Q. Gui

Guideng Research and Technology, Vancouver, British Columbia, Canada

B. M. DeTracey

Bedford Institute of Oceanography, Ocean Sciences Division, Department of Fisheries and Oceans, Dartmouth, Nova Scotia, Canada

(Manuscript received September 24, 1996, in final form August 28, 1997)

DOI: 10.1175/1520-0485(1998)028<1152:BROTLN>2.0.CO;2

ABSTRACT

The barotropic response of the Labrador and Newfoundland shelves to a moving storm over the Labrador Sea is investigated using a linear barotropic ocean model with realistic coastline and topography. The model results show that the storm generates motions of different time–space scales. Four types of motions are identified:directly wind-forced motion, shelf waves with distinctive frequency and wavelength, low-frequency shelf waves, and trapped inertio–gravity waves. The strongest currents are directly wind-forced currents occurring in areas of maximum wind stress over the shelf. The spatial pattern and temporal change of the current field are strongly influenced by the time history of the storm and the geometry of the coastline. Continental shelf waves are generated in the shelf region south of the storm track. Maximum amplitude occurs along the shelf edge at a wavelength of 800 km and a period of 20 h. This wavelength and period are close to the maximum frequency point of the dispersion curve for the first-mode shelf waves. On the northeast Newfoundland shelf and Grand Banks, the most energetic motion is associated with low-frequency shelf waves with no definitive frequency and wavelength. The currents are rectilinear and parallel to the bathymetry contours at the shelf break and clockwise circular in the shelf interior. Inertio–gravity waves with signatures in both current and sea surface elevation are trapped in the northern Labrador Sea and the Davis Strait. The implications of the model results for current observation on the shelf are discussed.

1. Introduction

Previous model studies and observations of oceanic response to a moving storm show that the types of motion that can be generated by the storm are dependent on the speed of the storm and the geometry, topography, and stratification of the ocean. In a stratified ocean without a lateral boundary, the most energetic motion is baroclinic inertial oscillation (Price 1983; de Young and Tang 1990; Shay et al. 1992). Barotropic inertial motion is prohibited because of a mismatch between the phase speed of barotropic inertial waves and the storm speed (Geisler 1970). The barotropic response to a moving storm is nonoscillatory, that is, alongtrack currents on each side of the storm track in opposite directions (e.g., Ginis and Sutyrin 1995). On the continental shelf, the effects of the coast and topography can generate motions not realizable in an infinite ocean: coastal jets, continental shelf waves, and inertio–gravity waves (Wang 1975; Mysak 1980; Gordon and Huthnance 1987).

Idealized continental shelves have been used in several models to study the oceanic response to moving storms (Gjevik 1991; Slørdal et al. 1994). A simplified ocean allows an in-depth analysis of the response, but lacks realism when used in direct data comparison. On the other hand, simulation models with realistic oceans and meteorological fields have been developed and used to study the response of coastal oceans to hurricanes (Cooper and Thompson 1989; Ly and Kantha 1993). These studies focus on the understanding of maximum currents on timescales of less than a day and nonlinear interaction between hurricane-induced currents and the Loop Current. A problem in using realistic forcing to study ocean variability is that the results are sometimes difficult to interpret, even when the simulation is good (Tang and Gui 1996). The reason is that a complex forcing field can generate motions of different time–space scales at the same time. The oceanic response at a given location is a superposition of all the motions and, thus, is not always easy to separate and identify.

In this paper, we use a model storm to generate barotropic motions on the Labrador and Newfoundland shelves. The motivation of the work is some intriguing observations in a recent study of variable currents on the northern Grand Banks (DeTracey et al. 1996). The data showed that at the shelf break the currents were predominantly barotropic and rectilinear with directions parallel to the bathymetry contours and were completely incoherent with the local winds. This suggests that there are motions generated by remote meteorological forces in the form of traveling waves that cannot be accounted for by local wind forcing. Over the Labrador Sea, the most energetic meteorological forces in winter and spring are associated with storms. Storm-generated motions are thus expected to have the greatest influence on the time-varying current field, sea level, and ice motion over the Labrador and Newfoundland shelves.

The objective of the paper is to gain a better understanding of the barotropic motions generated by storms over the Labrador Sea with an aim to interpret data collected on the Labrador/Newfoundland shelf and to design future field experiments. The wind-driven motions dealt with in this paper such as coastal jet and continental shelf waves have been studied by oceanographers over the past 40 years. The emphasis of this paper is to identify the different types of motion generated by a storm and to investigate the patterns, properties, amplitudes, and locations of the motions in relation to the storm. We hope the results of the investigation will help to clarify questions such as: What are the dominant motions in different parts of the Newfoundland/Labrador shelf? What is the explanation for features of variable currents in some data records that cannot be explained by a simple theory of wind-driven circulation? Where should instruments be deployed to detect a certain type of motion?

The storm and ocean models are described in sections 2 and 3 respectively. Section 4 presents a test case for an ocean of constant depth. The basic case with a realistic ocean is presented in section 5. The details of the oceanic response at selected locations are discussed in section 6. The effect of changing the storm speed is investigated in section 7. An analysis and interpretation of the model results are given in section 8. Some observations from other areas related to the model results are discussed in section 9. Section 10 summarizes the findings of the paper and discusses the implications of the results for current measurements on the Labrador/Newfoundland shelf.

2. Moving storm model

A typical storm over the Labrador Sea has a diameter of 500 km and moves from southern Labrador or northern Newfoundland toward Greenland in a northeastward direction at a speed of 8 m s^{-1} (Tang and Belliveau 1994). Storms occur more frequently in winter and spring, about one every 3 to 5 days, than in summer. As they move across the Labrador Sea, their intensity decreases. Some disappear before reaching the coast of Greenland and some veer southeastward. In this paper, a storm is assumed to move in a straight line from southern Labrador to the northeast of Greenland. The passage of the storm over Greenland is not expected to create unwanted motions in the Labrador/Newfoundland shelf since a storm over land has little effect on the distant coastal ocean.

The storm can be described by a pressure distribution of the form (O'Brien and Reid 1967)

$$P(x, y, t) = P_0 + (P_n - P_0) \exp(-R/r), \quad (1)$$

where P_0 is the pressure at the storm center, P_n is the background pressure, R is a parameter defining the size of the storm, and r is the distance from the storm center.

The radial and tangential velocities of surface wind, V_r and V_θ respectively, can be parameterized by the following equations:

$$V_r = -0.7V\beta \sin\alpha,$$

$$V_\theta = 0.7V\beta \cos\alpha,$$

where α is the inflow angle (the angle between the wind vector and the tangent to the local isobar); β is an empirical function of r,

$$\beta = (1 + d^2/r^2)^{-1}$$

in which d (=5.088 km) is a distance scale; and V is the gradient wind calculated from the pressure distribution by (Gill 1984):

$$V(r) = -\frac{1}{2}fR + \left(\frac{1}{4}f^2R^2 - \frac{R}{\rho_a}\frac{\partial P}{\partial r}\right)^{1/2},$$

where ρ_a is the air density and f is the Coriolis parameter.

In the open ocean, the wind speeds of a storm on the right-hand side of the storm track can be higher than those on the left-hand side because of the effect of the translational speed of the storm. In the Labrador Sea, asymmetry in the wind field can often be seen in analyzed wind data, but it is not obvious that the speeds on the right side of the track are always higher than those on the left side. The wind field may be influenced more by other factors, such as the location of the coastline relative to the storm, than by the translational speed of the storm. In this paper, we use a model storm that is symmetric in pressure and wind velocity.

In all cases considered in this paper, R = 120 km, P_n = 101.3 kPa, and P_0 = 94.0 kPa are used. These parameter values are based on analyzed sea level pressure data produced by the Canadian Meteorological Centre and the European Centre for Medium-Range Weather Forecasts, and represent typical values for a winter storm over the Labrador Sea. The inflow angle α is set at 35°. This value has been used for hurricane models (O'Brien and Reid 1967) but may be too large near the storm center. A model run with α = 10° was made to determine the sensitivity of the oceanic response to change in the inflow angle. The results showed no discernible difference from the basic case calculated with α = 35° (section 5). The distribution of pressure and tangential and radial wind stress, calculated with a constant drag coefficient of 1.3×10^{-3}, across the storm is shown in Fig. 1.

3. Ocean model

A linear barotropic model similar to that in Greenberg (1983) is used for the ocean. The vertically averaged velocity **u** and sea surface elevation ζ obey the following equations:

$$\frac{\partial \mathbf{u}}{\partial t} + f\mathbf{k} \times \mathbf{u} = -g\nabla\zeta - \frac{1}{\rho}\nabla P + \frac{1}{\rho H}(\tau_0 - \tau_b) + A_H\nabla^2\mathbf{u},$$

$$\frac{\partial \zeta}{\partial t} + \nabla \cdot (H\mathbf{u}) = 0,$$

where τ_0 and τ_b are wind stress and bottom stress calculated from wind velocity and **u** using quadratic relation with

constant drag coefficients of 1.3×10^{-1} and 2.5×10^{-3} respectively; A_H is the horizontal eddy coefficient. A constant value of 1000 m^2 s^{-1} is used in all calculations. Different values of the drag coefficients and the eddy coefficient have been used in test runs of the model, which showed that other than some small changes in the magnitudes, the main features of the current and elevation fields were basically the same as those in the basic case (section 5).

The model domain, bathymetry, and the storm track are shown in Fig. 2. A large area of the northwest Atlantic is included in the model domain in order to ensure that the influence of the open boundaries is not felt in the shelf region, which is the area of interest of this paper. A solid wall is placed at the northern boundary and the Hudson Strait is closed. The effects of opening the Hudson Strait will be discussed in section 8d. For the three open boundaries, we experimented with different types of boundary conditions. The most satisfactory results were obtained when radiation conditions were applied to the western and eastern boundaries and zero normal velocity and zero-adjusted sea level conditions were applied to the southern boundary. The radiation conditions minimize reflection of inertio–gravity waves at, but allow normal flows through, the boundaries. The southern boundary is located in an area of great water depth close to the storm, and hence the zero normal velocity and zero-adjusted sea level conditions, which are the first-order solutions to the equations, are appropriate. Test runs show that high-frequency oscillations sometimes appear at the open boundaries. But these oscillations are weak, incoherent (different locations in different runs), and occur in areas far away from our area of interest, and thus had no effect on the main results of the paper.

A Cartesian coordinate system with a C grid of size 20 km is used in finite differencing, and a time step of 60 s is used in time integration. The ocean velocities are set to zero initially.

4. Ocean with a flat bottom

The barotropic response of an ocean of constant water depth and infinite extent to a moving storm has been investigated by many authors (e.g., Ginis and Sutyrin 1995). The circulation pattern is a flow in the direction of the storm track on the right-hand side of the storm and an opposite flow on the left-hand side. A cross-flow at the leading front of the storm connects the two alongtrack flows. In order to compare our model to the previous studies and to determine the influence of the coast on the response, we consider a case with realistic coastline and a constant water depth of 200 m.

Figures 3 and 4 show the sea surface elevation (SSE) and current field at day 1 and day 2 when the storm center, moving at a constant speed of 8.5 m s^{-1}, is at the Labrador shelf and the west Greenland coast respectively. In these figures and similar figures in the following sections, only results in the western half of the model domain are shown since the eastern half contains no information of interest to us.

Directly under the storm is a SSE maximum caused by the inverted barometer effect. The geometry of the coastline gives rise to a local SSE maximum around the southern Newfoundland coast (Fig. 3). In the wake of the storm, a depression in SSE is developed (Fig. 4). The current field at day 1 shows strong currents around southern Newfoundland (Fig. 3) and in the area under the storm. At day 2, the circulation resembles that of an infinite ocean except that the effect of the coast forces the current to turn northwestward at the Greenland side and southeastward at the Labrador side of the Labrador Sea (Fig. 4). In summary, the coastline geometry has a strong effect on the circulation on the shelf. In the open Labrador Sea, the results are similar to those from models of infinite ocean in previous studies.

5. Basic case

A basic case with realistic topography and a storm moving at a speed of 8.5 m s^{-1} is considered in this section. As the storm center moves from the northeastern Gulf of St. Lawrence toward the Labrador Sea, the rise in the SSE radiates from the storm center outward (Fig. 5). In the northern Labrador Sea and the Davis Strait, a distinctive feature apparently tied to the geometry of the coastline appears. Associated with this feature in SSE is an area with relatively strong currents, which move mainly in the north–south direction. A coastal current hugging the shore of southern Labrador and northern Newfoundland starts to develop. The currents on the northeastern Grand Banks tend to follow the topography.

When the storm center moves to the shelf, strong currents are developed in two areas: a cyclonic eddy directly under the maximum wind stress (Fig. 6) and a northward flow with a width of about 80 km along the coast from mid-Newfoundland to southern Labrador. Farther south of the storm center, the currents at the northeastern edge and interior of the Grand Banks flow in the northward and eastward directions respectively. Such a pattern continues until the storm center moves to the central Labrador Sea (Fig. 7). The currents along the southern Labrador coast change to a southward flow, and a southward current develops off the southern Newfoundland coast.

At day 2, the storm center reaches the western Greenland coast (Fig. 8). An eddylike feature is developed off the southern Labrador coast. The currents south of 51°N have the spatial scale of the shelf. On the central and western Grand

Bank, the current flows southward, then turns westward, which is opposite in direction to the current 16 h earlier (Fig. 7). On the shelf north of the storm track, the currents are much weaker than those south of the storm track. Currents with amplitudes greater than 0.1 m s^{-1} appear only in the nearshore areas from 55° to 57°N.

By day 3, the storm has moved out of the Labrador Sea (Fig. 9). The currents on the shelves, the Grand Banks area in particular, are much weaker than those on the previous days. The only area with relatively strong currents is the shelf edge south of the storm track, where the current field shows a wavy pattern.

6. Temporal variation

To identify the motions generated by the storm, it is useful to examine the temporal change of the currents and SSE in different geographic locations (see Fig. 2 for location of sites 1–5). Since currents on the Labrador Shelf north of the storm track and in the open ocean are much weaker than those south of the storm track, we will focus our attention on the shelf areas south of the storm track.

a. Near shore

The strong coastal current off the southern Labrador and northern Newfoundland shore is characterized by a horizontal scale of 80 km and a timescale of 1 day. The time series plot of the wind and current at site 1 (Figs. 10a,b) shows that the strongest current occurs during passage of the storm over the shelf. After the storm, a weak oscillatory motion is developed with a peak frequency of 1.06 cpd (Fig. 10d). The SSE, on the other hand, does not have a dominant frequency (Figs. 10c,e).

b. Hamilton Bank (site 2 in Fig. 2)

In the offshore area under maximum wind stress, a directly wind-forced current is generated (Fig. 6). This current has a maximum speed of 0.14 m s^{-1} and flows in a direction slightly to the right of the wind vector (Figs. 11a,b) during the storm. After the storm, a strong clockwise oscillatory motion similar to that at site 1 but much stronger is developed, which has a peak frequency of 1.2 cpd and lasts for more than 15 days (Figs. 11b,d). Despite the strong signal in current, the SSE does not have a corresponding maximum in the spectrum (Figs. 11c,e).

c. Grand Banks

Farther south from the storm track, the current pattern changes gradually from the dominant mode of 20-h oscillation to longer period oscillations. Figures 12 and 13 show the time series and spectra of current and SSE at the edge, site 3, and interior of the Grand Banks, site 4, respectively. The currents are not directly correlated with the local wind. They oscillate on a timescale of 3 days and greater but do not have dominant frequency. The major difference between sites 3 and 4 is that at the shelf edge (Fig. 12) the clockwise and counterclockwise components have similar magnitudes, which implies that the motion is rectilinear in the direction of the bathymetry contours (see Fig. 2), while in the shelf interior (Fig. 13), the clockwise component is much greater than the counterclockwise component, indicating that the current rotates clockwise and has no preferred direction.

d. Davis Strait

Currents and SSE in Davis Strait and the northern Labrador Sea exhibit a behavior significantly different from those on the southern shelf. Both the current and sea surface elevation spectra show prominent peaks at 1.8 and 2.5 cpd with corresponding periods of 13.3 and 9.6 h (Figs. 14d,e). The clockwise and counterclockwise components of the current spectrum are almost equal, implying rectilinear currents. These spectral peaks also appear in the spectra of other areas (Figs. 10–13) but at a much lower level.

A close examination of Fig. 14c shows that the high-frequency motion (period 9.6 h) occurs mainly in the early part of the time series. After day 7, the oscillation becomes quite regular with a single period of 13.3 h. It is tempting to identify the peak at 1.8 cpd as the inertial oscillation (1.812 cpd at 65°N). But the 1.8-cpd peak also appears in the spectra for the Grand Banks (Fig. 13) where the inertial frequency is 1.414 cpd. Furthermore, inertial oscillations are always circular and counterclockwise, while Fig. 14 shows the current to be rectilinear. The nature of these high-frequency oscillations will be investigated in section 8.

7. Slow storm

The speed of storms over the Labrador Sea ranges from 4 to 10 m s^{-1}. To investigate the effect of speed on the oceanic

response, we consider a case in which the translational speed of the storm is reduced to one-half of the value used in the basic case, that is, 4.25 m s^{-1}.

Figures 15, 16, and 17 show the time series and spectra at sites 1, 2, and 4 respectively. In comparison with the basic case (Fig. 10), the coastal current (Fig. 15b, day 0–2) is stronger and the 20-h oscillation is much weaker (Figs. 16b,d). The onset of the oscillation is delayed until about day 2.5. On the Grand Banks where low-frequency currents dominate, the pattern of the current variation (Fig. 17) is similar to that of the basic case (Fig. 13), but there is a 1-day lag between the basic case and the slow storm case, and the amplitude is larger in the slow storm case. The 1-day lag between the two cases corresponds to the difference in time of the storm passage over the shelf.

The 1-day lag is confirmed by comparing the current fields. The currents on day 3 in the slow storm case (Fig. 18) have a similar pattern as those on day 2 in the basic case (Fig. 8), although the storm is at a different position. From the comparison between the basic and slow storm cases, we conclude that the important factor in the development of the current field is the duration of the storm over the shelf. The relationship between the magnitude of the currents and the storm speed will be discussed in the next section in the context of shelf waves.

8. Discussion

The model results show that a moving storm over the Labrador Sea can generate motions of different time and spatial scales. These motions can be classified as follows.

a. Directly wind-forced currents on the shelf

During the passage of the storm over the shelf, strong currents are generated along the coast of southern Labrador and northern Newfoundland and in the area of maximum wind stress (Fig. 6). The flow pattern is determined not only by the instantaneous distribution but also the time history of the wind field. Figure 19 shows the current field at 2-h intervals near the storm center.

When the storm moves from land to sea (Figs. 19a,b), the currents generated are alongshore and are greater south of the storm than north of the storm. This asymmetry is related to the geometry of the coastline. There is a larger area under wind forcing in the south than in the north, and the coast is roughly parallel to the wind direction in the south but almost perpendicular in the north. When the storm center reaches the shelf edge (Figs. 19c,d), the current southeast of the storm center turns eastward and a southward coastal current is developed north of the storm center, which reinforces the eastward current in the south. The coastal current increases with decreasing storm speed (Fig. 15). This is due to the fact at a given location a slow storm exerts stress and pressure gradient on the sea surface for a longer time than does a fast storm.

Because of the influence of the coastline, the topography, and the time history of the wind field, there is no simple relationship between the current and the wind, except the general conclusion that currents on the shelf are expected to be strong when winds are strong. Figures 19c,d indicate that the strongest correlation between wind and current occurs at the wind maximum southeast and west of the storm center. At certain locations (e.g., 54°N, 55°W in Figs. 19c,d), there is a convergence of currents. In certain shelf areas (e.g., 53°N, 53°W, 55.5°N, 57.5°N in Fig. 19c), the current is perpendicular to the wind.

b. Topographic waves

The 20-h oscillation found at site 2 (Fig. 11) is present in most of the shelf areas south of the storm track. The velocity spectra have the common feature of a peak in the clockwise component centered at 1–1.2 cpd. The strongest oscillation occurs south of the storm track in the area of maximum wind speed. The amplitude decreases toward the south and becomes very small at the northern Grand Banks. Across the shelf, the amplitudes peak at the shelf break between the 250-m and 350-m isobaths and decrease toward the coast. North of the storm track, the oscillation is weak and incoherent.

To determine the properties of the oscillations, a coherence analysis was performed between pairs of points at the shelf break (see Fig. 2 for location). In the calculation, data for the first two days were deleted to minimize the contribution from direct wind forcing. Figure 20 shows the velocity coherence squared (upper panel) and phase difference (lower panel) of the pair as a function of separation at 1.2 cpd. All pairs are highly coherent and the phase is a linear function of separation. A linear fit of the phase gives a slope of -0.452 ± 0.022 deg km^{-1}, which corresponds to a southward phase speed of 11 m s^{-1} and a wavelength of 800 ± 40 km. The wave pattern at the shelf break shown in Fig. 9 reflects this wavelength.

The facts that 1) the oscillation is a southward traveling wave with maximum amplitude at the shelf break, 2) the currents rotate clockwise, and 3) the oscillations have weak signals in SSE but strong signals in velocity (i.e., nondivergent flow) suggest that the motion is associated with a shelf wave. The dispersion relation of shelf waves can be determined from a given topographic profile. We used a computer program written by Brink and Chapman (1985) to compute the dispersion relation of the shelf wave. Figures 21a,b show the bottom profile at two sections on the southern Labrador shelf (see Fig. 2 for location) and the corresponding dispersion curves for the first mode of the shelf wave. In the calculation, a cutoff water depth of 3500 m was used, and the x coordinate for section B was multiplied by a factor, cos20°, to take into account that the bathymetry contours off southern Labrador are at an angle of 20° from the ocean model y axis.

The frequency and wavenumber obtained from the coherence analysis are also shown in Fig. 21b (the cross). The error bars in frequency and wavenumber correspond to the band width of the spectra and the error the linear fit of Fig. 20, respectively. The frequency and wavenumber derived from the model results lie approximately at the maximum frequency of the dispersion curve, implying a group velocity of zero. This explains why there is a dominant frequency at the shelf break and that the oscillation persists long after the storm has moved away.

c. Low-frequency currents

On the Grand Banks and southern northeast Newfoundland shelf, currents of timescales of 4–8 days and a spatial scale of the shelf width are the dominant feature of the current field (Figs. 6–9, 12–13). The currents appear to be influenced by the topography, but the direction, frequency, and velocity field have no consistent patterns and obvious relationship with the wind. A common feature of the low-frequency currents is that they are rectilinear in the direction of the topography contours at the shelf break (Fig. 12) but have no preferred direction in the shelf interior (Fig. 13).

A possible explanation for these currents is that they are low-frequency shelf waves. The dispersion curve of the shelf waves (Fig. 21b) indicates that the low-frequency (frequencies less than the maximum frequency) waves have long wavelengths and high group velocities. When the storm passes the shelf, shelf waves of all frequencies are generated. The low-frequency waves reach the Grand Banks in one day because of their high group velocities (1000 km d^{-1}). They last for a few cycles and then disappear. Owing to the long wavelength and the complicated coastline and topography of the southern shelf, no coherent wave with a definitive wavelength and frequency can be extracted from the current field. On the other hand, the wave at the maximum possible frequency has a shorter wavelength and zero group velocity, which favor a wave train to form along the shelf and stay on the shelf (Fig. 11).

Further support for the shelf wave interpretation of the motion is that the wave at the maximum frequency has its maximum amplitude at the shelf break, while the low-frequency shelf waves have no obvious variation in the amplitude across the shelf (Fig. 21c). This agrees with the model results that the 20-h shelf wave peaks at the shelf break (Figs. 10, 11), while the low-frequency shelf waves (Figs. 12, 13) have a more uniform amplitude across the shelf.

A comparison of the model results between the slow storm and the basic cases shows that the 20-h shelf wave at the shelf break has a larger amplitude in the basic case than in the slow storm case, while the low-frequency waves on the Grand Banks have a smaller amplitude in the basic case than in the slow storm case. The change in amplitude with storm speed can be understood in terms of the timescale of the forcing field. The wind stress is exerted on the shelf for about 1 day in the basic case and about 2 days in the slow storm case. As a result, the 20-h wave can be excited more efficiently by the fast storm and the low-frequency waves can be excited more efficiently by the slow storm.

d. Trapped inertio–gravity waves

Wind and pressure gradient forces on the ocean can generate gravity waves of various types, which can be reflected and trapped by the coast. The high-frequency oscillations detected in the northern Labrador Sea and Davis Strait (Fig. 14) are most probably a manifestation of trapped inertio–gravity waves. Several investigators have studied trapped waves in a semienclosed channel (see references in LeBlond and Mysak 1978). They show that the wave motion is a superposition of an incident Kelvin wave, a reflected Kelvin wave, and a sum of Poincare waves with nodal points in the interior of the channel and maximum amplitude around the walls.

Hourly plots (not presented) of SSE show that during the first 5 days the feature off the west Greenland coast in Fig. 5 appears every 10 h and travels counterclockwise along the northern boundary to reach the northern Labrador coast. This feature shows up in the time series plot and spectra of site 5 as a peak at 2.5 cpd. After 5 days, the SSE and current become more monochromatic with a spectral peak at 1.8 cpd. These oscillations also appear, albeit much weaker, in other parts of the shelf.

The resonant frequencies and wave patterns of inertio–gravity waves depend on the geometry of the coastline and topography of an enclosed or semienclosed basin. To test the sensitivity of inertio–gravity waves to the coastline geometry, a model run was made in which the Davis Strait was open and a radiation boundary condition was applied across the strait.

The results show that the peak frequencies are changed from 1.8 and 2.5 cpd to 2 cpd, and the variance associated with the inertio–gravity waves is reduced. If the model domain includes the entire Fox Basin and Hudson Bay, resonant frequencies different from those found in both the basic case and the case with a northern radiation boundary condition are expected. Such high-frequency inertio–gravity waves are difficult to extract from current meter or tide gauge records. The currents associated with the waves are much smaller than the other types of motion discussed in this paper.

9. Comparison with observations in other areas

The along-isobath low-frequency currents discussed in the previous section have been reported by serveral investigators. On the Scottish continental shelf, Gordon and Huthnance (1987) observed that the along-isobath currents flowed as long as the wind blew and stopped when the wind stopped. This is in agreement with the model result that the occurrence of the low-frequency flows is tied to the time of the passage of the storm over the shelf. The authors interpreted the observed currents as a low-frequency, low-wavenumber continental shelf wave in the nondispersive regime where the phase/group velocities were constant and high. Over the Oregon continental shelf, Cutchin and Smith (1973) found evidence of shelf waves from current and sea level data. In a narrow frequency band around 0.22 cpd, the data were consistent with the prediction of low-frequency continental shelf waves.

A continental shelf wave with a definitive frequency has been observed by Gordon and Huthnance (1987). They found currents near the shelf break rotated clockwise with a period of 23 h, which corresponded to the maximum frequency of the lowest dispersion curve of shelf waves.

10. Conclusions

The results of a linear barotropic ocean model show that motions of different time–space scales are generated by a moving storm over the shelf. From an examination of the spatial patterns and spectral characteristics of currents and sea surface elevation, four types of motions are identified: directly wind-forced current, shelf waves with a distinctive frequency and wavelength, low-frequency shelf waves, and trapped inertio–gravity waves. The strongest currents, of the order 0.15 m s^{-1}, are the directly wind-forced currents that appear in the area of maximum wind stress over the shelf and along the shore of northern Newfoundland and southern Labrador within 80 km from the coast. The continental shelf waves have a maximum amplitude, about 0.1 m s^{-1}, at the shelf edge south of the storm track, a wavelength of 800 km, and a period of 20 h. Low-frequency shelf waves characterized by a continuum in the energy spectra and current amplitudes of 0.05 m s^{-1} dominate the current field on the southern Newfoundland shelf and the Grand Banks. The currents are rectilinearly parallel to the bathymetry contours at the shelf break and clockwise circular in the shelf interior. Trapped inertio–gravity waves have distinctive signals in both velocity and SSE and are the dominant motion in the northern Labrador Sea and Davis Strait. The currents associated with the inertio–gravity waves are very weak.

The model results as summarized above suggest that observed currents in the shelf interior are composed of directly force currents coherent with local winds and low-frequency currents associated with low-frequency shelf waves, which rotate clockwise and have no preferred direction. Since the directly forced currents are inversely proportional to the water depth, the degree of coherence with winds will depend on location. Currents on the Grand Banks (average depth 90 m) are expected to have a higher coherence with winds than those on the northeast Newfoundland shelf (average depth 350 m). At the coast, strong coastal jets of width 80 km will develop when strong wind events pass the coast. At the shelf break, the directly forced currents are weak and thus not coherent with the local winds. The strongest currents are associated with shelf waves at the maximum frequency, which is 1.2 cpd along the edge of the northeast Newfoundland shelf. The currents rotate clockwise and the magnitudes increase with the speed of the weather system. Slightly weaker are the low-frequency currents associated with shelf waves in the several-day period range. These currents are rectilinear in the direction of the topography contours, and their magnitudes increase with decreasing speed of the weather system.

Some of the model predictions have been observed in a recent study of variable currents on the northern Grand Banks (DeTracey et al. 1996), such as low-frequency currents paralell to the isobaths at the shelf break and directly wind-forced currents on the Grand Banks. Coastal jets, shelf waves with definitive frequencies and trapped inertio–gravity waves are predicted to exist in other parts of the shelf region. Their observations require more data across the shelf and long-term data in Davis Strait.

Acknowledgments

This work was supported by the Panel of Energy Research and Development. We thank Ken Brink for making the computer program for calculating shelf wave dispersion relation available to us.

REFERENCES

Brink, K. H., and D. C. Chapman, 1985: Programs for computing properties of coastal-trapped waves and wind-driven motion over the continental shelf and slope. Woods Hole Oceanographic Institution Tech. Rep. WHOI-85-17, 99 pp. [Available from MBL/WHOI Library, 7 MBL Street, Woods Hole, MA 02543.].

Cooper, C., and J. D. Thompson, 1989: Hurricane-generated currents on the outer continental shelf: 1. Model formulation and verification. *J. Geophys. Res.*, **94,** 12 513–12 539..

Cutchin, D. L., and R. L. Smith, 1973: Continental shelf waves: Low-frequency variations in sea level and currents over the Oregon continental shelf. *J. Phys. Oceanogr.*, **3,** 73–82..

DeTracey, B. M., C. L. Tang, and P. C. Smith, 1996: Low-frequency currents at the northern edge of the Grand Banks. *J. Geophys. Res.*, **101,** 14 223–14 235..

deYoung, B., and C. L. Tang, 1990: Storm-forced baroclinic near-inertial currents on the Grand Bank. *J. Phys. Oceanogr.*, **20,** 1725–1741..

Geisler, J. E., 1970: Linear theory of the response of a two-layer ocean to a moving hurricane. *Geophys. Fluid Dyn.*, **1,** 249–272..

Gill, A., 1984: On the behavior of internal waves in the wakes of storms. *J. Phys. Oceanogr.*, **14,** 1129–1151..

Ginis, I., and G. Sutyrin, 1995: Hurricane-generated depth-averaged currents and sea surface elevation. *J. Phys. Oceanogr.*, **25,** 1218–1242..

Gjevik, B., 1991: Simulation of shelf sea response due to traveling storms. *Contin. Shelf Res.*, **11,** (2), 139–166..

Gordon, R. L., and J. M. Huthnance, 1987: Storm-driven continental shelf waves over the Scottish continental shelf. *Contin. Shelf Res.*, **7,** 1015–1048..

Greenberg, D. A., 1983: Modeling the mean barotropic circulation in the Bay of Fundy and Gulf of Maine. *J. Phys. Oceanogr.*, **13,** 886–904..

LeBlond, P. H., and L. A. Mysak, 1978: *Waves in the Ocean.* Elsevier Scientific, 602 pp..

Ly, L. N., and L. H. Kantha, 1993: A numerical study of the nonlinear interaction of Hurricane Camille with the Gulf of Mexico Loop Current. *Oceanol. Acta.*, **16,** 341–348..

Mysak, L. A., 1980: Topographically trapped waves. *Annu. Rev. Fluid Mech.*, **12,** 45–76..

O'Brien, J. J., and R. O. Reid, 1967: The non-linear response of a two-layer, baroclinic ocean to a stationary, axially-symmetric hurricane: Part 1. Upwelling induced by momentum transfer. *J. Atmos. Sci.*, **24,** 197–207.. Find this article online

Price, J. F., 1983: Internal wave wake of a moving storm. Part I: Scales, energy budget and observations. *J. Phys. Oceanogr.*, **13,** 949–965..

Shay, L. K., P. G. Black, A. J. Mariano, J. D. Hawkins, and R. L. Elsberry, 1992: Upper ocean response to Hurricane Gilbert. *J. Geophys. Res.*, **97,** 20 227–20 248..

Slørdal, L. H., E. A. Martinsen, and A. F. Blumberg, 1994: Modeling the response of an idealized coastal ocean to a traveling storm and to flow over bottom topography. *J. Phys. Oceanogr.*, **24,** 1689–1705..

Tang, C. L., and D. J. Belliveau, 1994: Vertical structure of currents on the northern Grand Bank: A view from a bottom mounted acoustic Doppler current profiler. *Contin. Shelf Res.*, **14,** 1331–1347..

— , and Q. Gui, 1996: A dynamical model for wind-driven ice motion: Application to ice drift on the Labrador Shelf. *J. Geophys. Res.*, **101,** (C12), 28343–28364..

Wang, D.-P., 1975: Coastal trapped waves in a baroclinic ocean. *J. Phys. Oceanogr.*, **5,** 326–333..

Figures

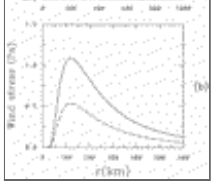

Click on thumbnail for full-sized image.

Fig. 1. (a) Barometric pressure and (b) wind stress as a function of distance from the storm center. The solid line is tangential stress and the dashed line is radial stress.

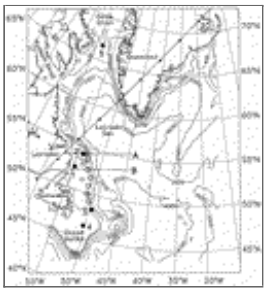

Click on thumbnail for full-sized image.

Fig. 2. Model domain and bathymetry. Solid circles, numbered 1 to 5, denote the sites used in Figs. 10–14. Open circles are pairs used in the coherence analysis of Fig. 20. Dashed lines are the sections for the bottom profile of Fig. 21. The storm track is indicated by the straight line with small solid squares marking the storm center at 12-h intervals (for a storm with a speed of 8.5 m s^{-1}). Bathymetry contours plotted are 200, 400, 1000, 2000, and 4000 m.

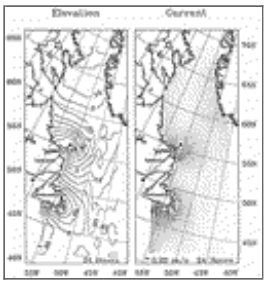

Click on thumbnail for full-sized image.

Fig. 3. Sea surface elevation and current for the flat bottom case at 1 day. Fig. 4. As in Fig. 3 but at 2 days.

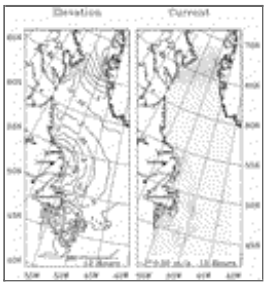

Click on thumbnail for full-sized image.

Fig. 5. Sea surface elevation and current for the basic case at 12 h.

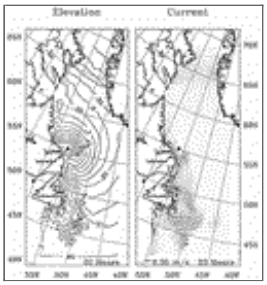

Click on thumbnail for full-sized image.

Fig. 6. As in Fig. 5 but at 22 h. Fig. 7. As in Fig. 5 but at 32 h.

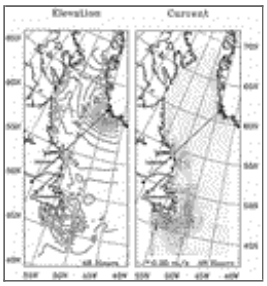

Click on thumbnail for full-sized image.

Fig. 8. As in Fig. 5 but at 2 days. Fig. 9. As in Fig. 5 but at 3 days.

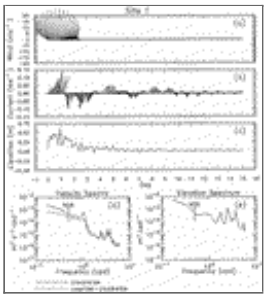

Click on thumbnail for full-sized image.

Fig. 10. Time series of (a) wind, (b) current, (c) sea surface elevation, and spectra for (d) current and (e) sea surface elevation at site 1 (see Fig. 2 for location).

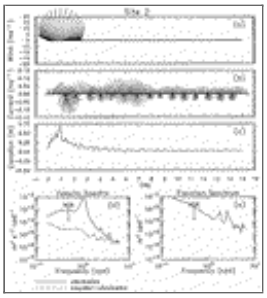

Click on thumbnail for full-sized image.

Fig. 11. As in Fig. 10 but at site 2.

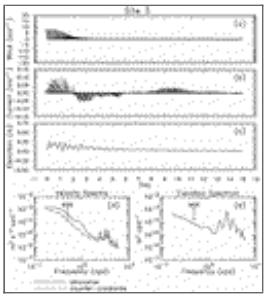

Click on thumbnail for full-sized image.

Fig. 12. As in Fig. 10 but at site 3.

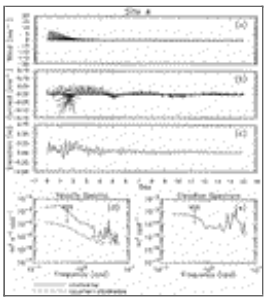

Click on thumbnail for full-sized image.

Fig. 13. As in Fig. 10 but at site 4.

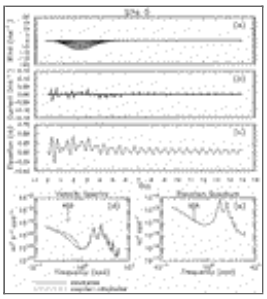

Click on thumbnail for full-sized image.

Fig. 14. As in Fig. 10 but at site 5.

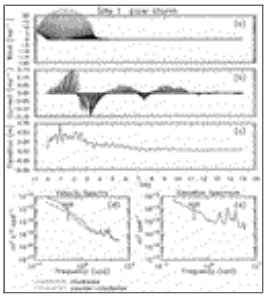

Click on thumbnail for full-sized image.

Fig. 15. Time series of (a) wind, (b) current, (c) sea surface elevation, and spectra for (d) current and (e) sea surface elevation at site 1 (see Fig. 2 for location) for the slow storm case.

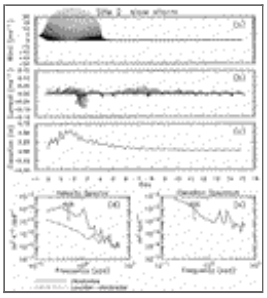

Click on thumbnail for full-sized image.

Fig. 16. As in Fig. 15 but at site 2.

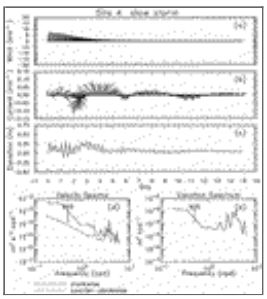

Click on thumbnail for full-sized image.

Fig. 17. As in Fig. 15 but at site 4.

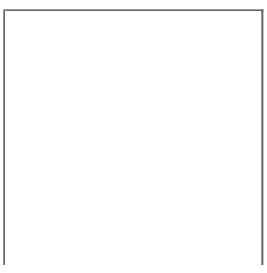

Click on thumbnail for full-sized image.

Fig. 18. Sea surface elevation and current for the slow storm case at day 3.

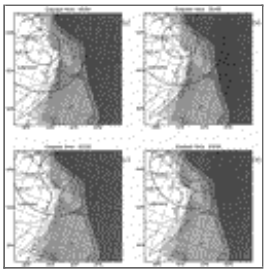

Click on thumbnail for full-sized image.

Fig. 19. Current field at 2-h intervals. The small circle denotes the radius of maximum wind stress. The large circle denotes the radius of half of the maximum wind stress.

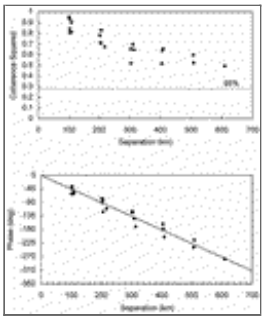

Click on thumbnail for full-sized image.

Fig. 20. (a) Coherence squared and (b) phase of coherence for pairs in Fig. 2 as a function of pair separation.

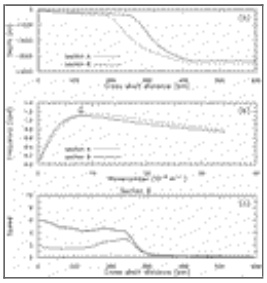

Click on thumbnail for full-sized image.

Fig. 21. (a) Bottom profile of two cross-shelf sections in the southern Labrador (location in Fig. 2) and (b) dispersion relation. The cross is from coherent analysis of model results. (c) Current speed (arbitrary unit) as a function of off-shore distance for section B for (i) ω = 1.1 cpd, $k = 7.85 \times 10^{-6}$ m^{-1} (light solid line); (ii) ω = 0.6 cpd, $k = 0.21 \times 10^{-1}$ m^{-1} (heavy solid line).

Corresponding author address: Dr. Charles C. Tang, Department of Fisheries and Oceans, Ocean Sciences Division, P.O. Box 1006, Bedford Institute of Oceanography, Dartmouth, NS B2Y 4A2 Canada.

E-mail: ctang@emerald.bio.dfo.ca

top